Check for updates

Realization of Mg^{2+} intercalation in a thermodynamically stable layer-structured oxide†

Junhao Zhang,[ab] Haotian Guan,[ab] Jili Yue, ID *[ab] Yangfan Lu, ID [ab] Qian Li,[ab] Guangsheng Huang,[ab] Jingfeng Wang,[ab] Baihua Qu*[ab] and Fusheng Pan[ab]

Magnesium batteries have emerged as one of the considerable choices for next-generation batteries. Oxide compounds have attracted great attention as cathodes for magnesium batteries because of their high output voltages and ease of synthesis. However, a majority of the reported results are based on metastable nanoscale oxide materials. This study puts forward a thermodynamically stable layer-structured oxide $K_{0.5}MnO_2$ with an enlarged lattice spacing as a model cathode material employing optimized electrolytes, enabling Mg^{2+} intercalation into the $K_{0.5}MnO_2$ framework in a real magnesium battery directly using Mg foil as the anode. First-principles calculations implied that the enlarged layer spacing could decrease the migration energy barrier of Mg^{2+} in the layered oxide. This work can pave the way to understanding the fundamental intercalation behavior of Mg^{2+} in magnesium batteries.

Introduction

Magnesium batteries are considered as a promising next-generation electrochemical energy storage technology because of the high volumetric capacity (Mg: 3833 mA h cm^3), abundance of Mg resources, and lower tendency of forming dendrites.[1-8] However, the high charge density of Mg^{2+} leads to strong coulombic interactions with the host framework, making Mg^{2+} intercalation into many host materials difficult. The first magnesium battery prototype was achieved using a Chevrel-phase Mo_6S_8 as the cathode, in which Mg^{2+} could be intercalated reversibly with relatively fast kinetics in the three-dimensional channels.[9] This prototype promoted the research on magnesium batteries. However, this Mo_6S_8 cathode displayed low discharge voltage (about 1 V) with a low capacity of 75 mA h g^1, and the synthesis method was also time-consuming and complicated.[10-12]

Oxide compounds have attracted great attention because of their high output voltages and ease of synthesis.[13] The voltage profile and mobility of Mg^{2+} intercalation in a chromium oxide spinel ($Mg_xCr_2O_4$) as a cathode for magnesium batteries were studied by first-principles calculations; the results indicated that the stable Mg-vacancy orderings for the cathode compositions of $Mg_{0.33}Cr_2O_4$ and $Mg_{0.5}Cr_2O_4$ can severely limit Mg (de)

intercalation.[14,15] Kown *et al.* pointed out that spinels with a single redox metal, such as $MgCr_2O_4$ or $MgMn_2O_4$, were not found to demonstrate sufficiently reversible Mg^{2+} intercalation at high redox potentials when coupled with nonaqueous Mg electrolytes.[16-18]

Novak *et al.* reported that Mg^{2+} can be reversibly intercalated into α-V_2O_5, displaying a capacity of ~170 mA h g^{-1} using an acetonitrile electrolyte containing water.[19] Yu *et al.* also showed improvements in the capacity using a $Mg(ClO_4)_2$/polycarbonate (PC) system with water.[20] First-principles calculations showed the scenario of Mg^{2+} and H_2O co-intercalation in nanocrystalline Xerogel-V_2O_5; the remarkable Mg mobility was ascribed to the electrostatic shielding of divalent Mg^{2+} by the water molecules contained in the crystal structure.[21] Meanwhile, the realization of Mg^{2+} co-intercalation with H_2O into V_2O_5 using an electrolyte containing water was done in a three-electrode or two-electrode system with active carbon anode.[22,23] The presence of H_2O in the electrolyte or that coordinated with the Mg^{2+} caused passivation at the Mg anode. Son *et al.* built an artificial Mg^{2+}-conductive interphase on the Mg anode surface, enabling the reversible cycling of a Mg‖V_2O_5 full-cell in the water-containing carbonate-based electrolyte.[24] However, the Mg powder used in this work is difficult to handle and the procedure is complicated. Chromium oxides and vanadium oxides are toxic; thus, it is necessary to use environmentally-friendly oxides.

Manganese-based oxide is also a kind of promising cathode candidate for magnesium batteries because of the abundance of Mn resources and its environmental friendliness. Nam *et al.* reported that nanoscale layer-structured Birnessite-MnO_2 with crystal water can effectively screen the electrostatic interactions between Mg^{2+} and the host anions.[25,26] Wang *et al.*

[a]College of Materials Science and Engineering, National Engineering Research Center for Magnesium Alloys, National Innovation Center for Industry-Education Integration of Energy Storage Technology, Chongqing University, Chongqing, 400044, China. E-mail: jili.yue@cqu.edu.cn; bhqu@cqu.edu.cn

[b]Chongqing Institute of New Energy Storage Materials and Equipment, Chongqing, 401135, China

† Electronic supplementary information (ESI) available. See DOI: https://doi.org/10.1039/d4ra03923h

demonstrated similar results that crystal water in layer-structured Birnessite-MnO_2 with enlarged interlayer spacing could facilitate Mg^{2+} migration.[27] Unfortunately, they used Ag/AgCl as the reference electrode instead of Mg foil anode, which was not a real magnesium battery. Miralles *et al.* proved the insertion of Mg^{2+} in Mn_2O_3 electrodes through a spectroelectrochemical study using aqueous media with Ag/AgCl reference electrode.[28] Shimokawa *et al.* studied Mg-ion storage materials based on MnO_2 frameworks, while the MnO_2 polymorphs were metastable or nanoscale.[29]

To date, although several oxide systems have been investigated as cathode materials for magnesium batteries, the majority of the reported results are based on metastable nanoscale materials, H_2O or other molecules-inserted materials using a three-electrode system or active carbon anode (Table S1†). To demonstrate Mg^{2+} intercalation into a host and study the fundamental principles of Mg^{2+} intercalation, the model materials should satisfy the following conditions: (1) the host compound should be thermodynamically stable; (2) Mg foil can be directly used as the anode; (3) there exist vacancies in its crystal structure that permit Mg^{2+} intercalation. Herein, we utilized thermodynamically stable $K_{0.5}MnO_2$ as the cathode in optimized electrolytes, realizing Mg^{2+} intercalation into the $K_{0.5}MnO_2$ framework in a real magnesium battery directly using Mg foil as the anode, where a high specific capacity of 99 mA h g^1 was obtained at the first discharge at 10 mA g^1. This work can pave the way to understanding the fundamental intercalation behaviors of Mg^{2+} in magnesium batteries.

Results and discussion

Layer-structured transition metal oxides are not only suitable cathodes for commercial batteries but also an excellent platform to study various fundamental scientific issues.[30–34] Typically, it is reported that the first-cycle voltage hysteresis is determined by the superstructure in the cathode, specifically the local ordering of lithium and transition metal ions in the transition metal layers by comparing two closely related layer-structured transition metal oxide intercalation cathodes, namely, $Na_{0.75}[Li_{0.25}Mn_{0.75}]O_2$ and $Na_{0.6}[Li_{0.2}Mn_{0.8}]O_2$.[34] Inspired by this work, we selected thermodynamically stable A_xMnO_2 (A = alkali, such as Li, Na, and K) as model materials, which have similar layered structure with different interlayer spacing due to the different radius of A (Li$^+$ 0.76 Å, Na$^+$ 1.02 Å, K$^+$ 1.38 Å). Because layered Li_xMnO_2 is meta-stable and the value of x in Li_xMnO_2 is close to 1.0, there is no vacancy to accommodate Mg^{2+} ions.[35] There exist A-site vacancies in thermodynamically stable Na and K-containing layer-structured manganese oxide, which can be used to insert Mg^{2+} directly. Typical Na-deficient $Na_{0.67}MnO_2$ (abbreviated as NMO in the following part)[36] and K-deficient $K_{0.5}MnO_2$ (abbreviated as KMO in the following part)[37] were selected as the host framework to investigate the intercalation behaviors of Mg^{2+} ion.

Fig. 1 shows the characterization results of the as-prepared NMO and KMO. The XRD pattern of the as-synthesized KMO and NMO can be well indexed with PDF card no. 16-0205 and no. 27-0751. However, the crystallographic parameters of PDF
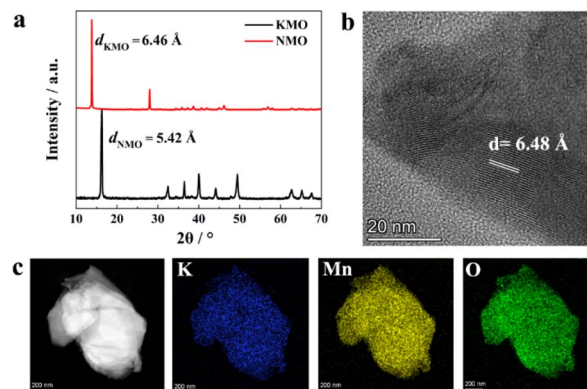

Fig. 1 Characterization of the as-prepared NMO and KMO. (a) XRD patterns of NMO and KMO, (b) HRTEM image of KMO, and (c) EDS mapping of KMO.

card no. 16-0205 are not included in the Inorganic Crystal Structure Database (ICSD) yet. According to the literature,[38–40] the crystallographic parameters of KMO[38,39] and NMO[40] are listed in Table S2 and S3,† respectively. The XRD pattern shows sharp peaks and a good match between the sample and the PDF card with almost no presence of spurious peaks, which not only indicates the good crystallinity of KMO and NMO but also the high purity of the sample. The first reflection peak in the X-ray diffraction (XRD) patterns represent the layer-spacing of layered-structure oxide,[31–33] according to the Bragg equation $2d \cdot \sin(\theta) = \lambda$, where a lower 2θ means larger layer spacing. As shown in Fig. 1a, the first reflection peak of KMO in the XRD patterns is located at lower 2θ than that of NMO; thus, KMO has a larger layer spacing distance. Calculated from the XRD patterns, the d-spacing of NMO (d_{NMO}) is 5.42 Å, and the d-spacing of KMO (d_{KMO}) is 6.46 Å. Fig. 1b shows the high-resolution transmission electron microscopy (HRTEM) result of KMO, showing the clear lattice strips with d-spacing of 6.48 Å, which is consistent with the XRD result. The larger d-spacing can weaken the interactions between Mg^{2+} and the MnO_2 host framework, facilitating Mg^{2+} migration; thus, Mg^{2+} can be intercalated into KMO. Fig. 1c shows the high-angle annular dark field (HAADF) energy dispersive spectrometry (EDS) mapping of KMO, indicating the homogeneous elemental distribution of K, Mn, and O. Fig. S1a and b† show the scanning electron microscopy (SEM) images of the as-synthesized NMO and KMO, respectively. Both materials show a distinct lamellar structure and have particle sizes ranging from about 1 to 3 μm. It implies that particle size is not the main factor affecting the electrochemical performances.

Density functional theory (DFT) calculations were applied to understand the migration energy barriers of Mg^{2+} in the alkali layers of NMO and KMO. The migration path of Mg^{2+} in NMO and KMO obtained by DFT-based climbing nudged elastic band (CI-NEB) method is shown in Fig. 2a and b. The interlayer distance of "O–Na–O" is 3.44 Å, and for "O–K–O", it is 4.43 Å. Fig. 2c shows the migration energy barriers of Mg^{2+} in the alkali layers of NMO and KMO calculated by the CI-NEB method. It is obvious that the migration energy barriers of Mg^{2+} in KMO is
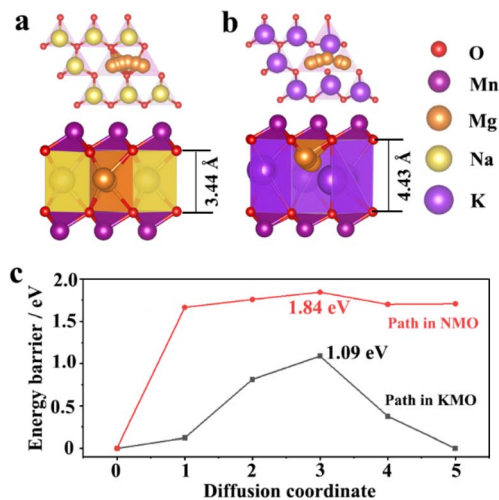
Fig. 2 Schematic diagrams of crystal structures of (a) NMO, (b) KMO; (c) the migration energy of Mg^{2+} in NMO and KMO.

lower than that in NMO, suggesting that increasing the layer spacing can promote Mg^{2+} migration.

In a previous report in the area of magnesium batteries, activated carbon was used as the anode, and the electrode potential of activated carbon will change, more like an asymmetric electrochemical capacitor.[38] In this work, NMO and KMO were tested in all-phenyl complex electrolyte (APC) and $MgCl_2/AlCl_3/Mg(TFSI)_2$ in dimethyl ether (DME) electrolyte (MACT) with magnesium foil as real magnesium batteries. Fig. S2† shows the linear sweep voltammetry curves of the APC and MACT electrolytes using the Mo electrode; the electrochemical stability window of APC and MACT are both more than 3.5 V *vs.* Mg^{2+}/Mg. Fig. 3 shows the electrochemical performances of NMO and KMO in real magnesium batteries at a current density of 10 mA g^1 between 1.0 and 3.1 V. The open circuit potential (OCP) of NMO in APC is 2.1 V, and the first discharge capacity of NMO in APC is only ~12 mA h g^1; there is still about 12 mA h g^{-1} capacity in the following cycles (Fig. 3a). The OCP of NMO in

MACT is 1.99 V; the first discharge capacity of NMO in MACT is only ~7.6 mA h g^{-1}, which decays to ~3 mA h g^1 at the 15th cycle. Although the capacities in the two electrolytes are slightly different, they both display little capacity decay. These results mean that Mg^{2+} can hardly intercalate into NMO (Fig. 3b). As shown in Fig. 3c, the OCP of KMO in APC is 2.07 V; the first discharge curve of KMO in APC displays two plateaus: the first one is located from 1.82 to 1.36 V with a capacity of 12 mA h g^1, following a discharge plateau from 1.35 to 1.0 V with a capacity of 74.2 mA h g^1, thus with a total capacity of 86.2 mA h g^1. The first charge capacity is 71 mA h g^1. The second discharge curve shows a voltage plateau from 1.5 to 1.0 V; the capacity of the second cycle is 41 mA h g^1, which decays to about 20 mA h g^1 in the 15th cycle. Fig. 3d shows the charge–discharge curves of KMO in MACT. The OCP of KMnO in MACT is 2.08 V, and the first discharge curve of KMO in MACT displays two plateaus as well. The first one is located from 1.85 to 1.33 V with a capacity of 22.87 mA h g^1, following a discharge plateau from 1.33 to 1.0 V with a capacity of 76.13 mA h g^1, with a total capacity of 99.0 mA h g^1. The capacity decays to about 36.8 mA h g^{-1} in the 15th cycle. Fig. S4† shows the cycle performance of KMO in MACT at 10 mA g^1; the capacity reaches 10.2 mA h g^1 in the 60th cycle. Though Mg^{2+} can be intercalated into KMO, it suffers from quick capacity fading, which needs to be improved by doping, coating and additives in electrolytes. Fig. S5† shows the cyclic voltammetry (CV) curve of KMO in MACT in the potential range of 1.0–3.1 V *vs.* Mg^{2+}/Mg at the scan rate of 0.1 mV s^1. The OCP is 2.03 V, which is close to the value in the galvanostatic charge/discharge curve. There is a hump from 1.8 to 1.1 V and a peak at about 1.5 V. These electrochemical curves imply that Mg^{2+} can be intercalated into KMO. Galvanostatic intermittent titration technique (GITT) test was performed to estimate the Mg^{2+} diffusion coefficient ($D_{Mg}{}^{2+}$), as shown in Fig. S6.† The values of $D_{Mg}{}^{2+}$ calculated at each interval were determined in the order of magnitudes ranging from 10^{-12} to 10^{10} cm^2 s^{-1}. The Nyquist plots obtained using electrochemical impedance spectroscopy (EIS) at the OCP for KMO are shown in Fig. S7;† the order of magnitude of $D_{Mg}{}^{2+}$ deduced from EIS is 10^{11} cm^2 s^1, which is in the range calculated from GITT.
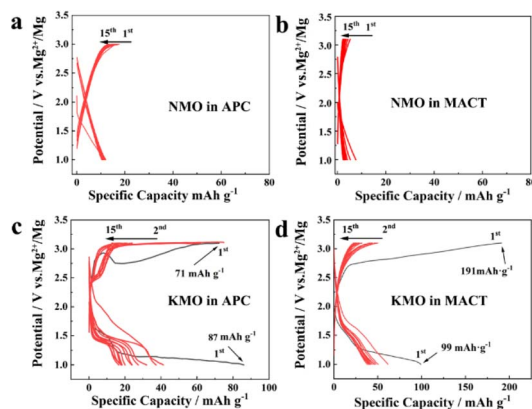

Fig. 3 Electrochemical performances of NMO and KMO in magnesium batteries. The galvanostatic charge/discharge curves of NMO in (a) APC and (b) MACT electrolytes. The galvanostatic charge/discharge curves of KMO in (c) APC and (d) MACT electrolytes.
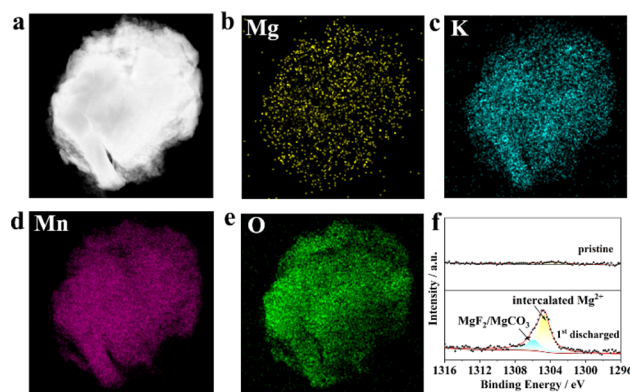

Fig. 4 (a) HAADF image and (b–e) EDS mapping of KMO after first discharge; (f) the Mg 1s core level XPS of KMO and KMO after first discharge.

Fig. 4a–e show the HAADF images and the corresponding EDS mapping of KMO in the completed state of the first discharge, from which we can clearly see the presence of Mg and the uniform distribution of the four elements K, Mn, Mg, and O. In addition, Fig. 4f displays the XPS spectra of the pristine KMO electrode and the state of first discharge in the binding energy range from 1296 eV to 1316 eV. It clearly shows a featured peak of the Mg 1s core level, which can be fitted into two peaks centred at 1306.01 and 1304.63 eV. The peak at 1306.01 eV could be dominated by $MgF_2/MgCO_3$ in the cathode electrolyte interface, which originated from the decomposition of the electrolyte.[41] The peak at 1304.63 eV could be characteristic of intercalated Mg^{2+} species in the discharge state. Fig. S3† shows the XRD patterns of the fully discharged and re-charged KMO electrodes; there exists obvious shifts in the first reflection peak for the discharged and re-charged states, implying the intercalation reaction mechanism. A new reflection peak emerges at 28.9°, which could be ascribed to MnO_2 (PDF. 72-1982), implying that part of KMO is degraded. Doping in the transition metal layer could improve the stability of KMO and mitigate capacity degradation. The above results show that Mg^{2+} can be successfully embedded into the KMO material during the discharge process, which is in good agreement with the previous charge–discharge curve.

Conclusions

In summary, we proposed a thermodynamically stable layer-structured oxide $K_{0.5}MnO_2$ as the cathode using the solid-state reaction method for magnesium-ion battery. The Mg-ion storage performance was then evaluated using it as the cathode for rechargeable magnesium-ion batteries, with a high specific capacity of 99 mA h g^{-1} at the first discharge state at 10 mA g^{-1}. This work demonstrated that the layer-structured oxide $K_{0.5}MnO_2$ as the cathode with larger lattice spacing enables reversible Mg^{2+} intercalation/deintercalation. Based on the above results, we believe that through reasonable optimization strategy, layer-structured oxides also have great development potential in real rechargeable magnesium-ion batteries while also providing new insights for exploring new and efficient cathode materials for magnesium-ion batteries.

Data availability

All relevant data are provided within the paper.

Author contributions

Junhao Zhang, Jili Yue, Baihua Qu conceived the project and wrote the manuscript with contributions from all authors. Haotian Guan, Yangfan Lu and Qian Li performed the calculations. Guangsheng Huang, Jingfeng Wang and Fusheng Pan supervised this project.

Conflicts of interest

There are no conflicts to declare.

Notes and references

1 S. Hou, X. Ji, K. Gaskell, P. F. Wang, L. Wang, J. Xu, R. Sun, O. Borodin and C. Wang, *Science*, 2021, **374**, 172–178.

2 F. Liu, G. Cao, J. Ban, H. Lei, Y. Zhang, G. Shao, A. Zhou, L. Z. Fan and J. Hu, *J. Magnesium Alloys*, 2022, **10**, 2699–2716.

3 X. Liu, A. Du, Z. Guo, C. Wang, X. Zhou, J. Zhao, F. Sun, S. Dong and G. Cui, *Adv. Mater.*, 2022, **34**, 2201886.

4 T. Mandai and M. Watanabe, *J. Mater. Chem. A*, 2023, **11**, 9755–9761.

5 T. Wen, Y. Deng, B. Qu, G. Huang, J. Song, C. Xu, A. Du, Q. Xie, J. Wang, G. Cui, D. Peng, X. Zhou and F. Pan, *ACS Energy Lett.*, 2023, **8**, 4848–4861.

6 X. Chen, L. Han, G. Zhao, L. Zhao, G. Gao, L. Yu, Y. Li, X. Shan, J. Li, X. Liu and G. Zhu, *Chem. Commun.*, 2024, **60**, 3067.

7 S. Li, J. Zhang, S. Zhang, Q. Liu, H. Cheng, L. Fan, W. Zhang, X. Wang, Q. Wu and Y. Lu, *Nat. Energy*, 2024, **9**, 285–297.

8 B. Zhang, J. Yue, D. Wang, H. Jia, G. Huang, J. Wang and F. Pan, *ACS Energy Lett.*, 2024, **9**, 1771–1776.

9 D. Aurbach, Z. Lu, A. Schechter, Y. Gofer, H. Gizbar, R. Turgeman, Y. Cohen, M. Moshkovich and E. Levi, *Nature*, 2000, **407**, 724–727.

10 E. Lancry, E. Levi, Y. Gofer, M. Levi, G. Salitra and D. Aurbach, *Chem. Mater.*, 2004, **16**, 2832–2838.

11 Y. Cheng, L. Parent, Y. Shao, C. Wang, V. L. Sprenkle, G. Li and J. Liu, *Chem. Mater.*, 2014, **26**, 4904–4907.

12 M. Mao, Z. Lin, Y. Tong, J. Yue, C. Zhao, J. Lu, Q. Zhang, L. Gu, L. Suo, Y. Hu, H. Li, X. Huang and L. Chen, *ACS Nano*, 2020, **14**, 1102–1110.

13 J. Zhang, X. Wang, H. Li, H. Zhang, Y. Zhang and K. Wang, *Adv. Funct. Mater.*, 2023, **33**, 2301974.

14 T. Chen, G. S. Gautam, W. Huang and G. Ceder, *Chem. Mater.*, 2018, **30**, 153–162.

15 I. D. Johnson, A. N. Mistry, L. Yin, M. Murphy, M. Wolfman, T. T. Fister, S. H. Lapidus, J. Cabana, V. Srinivasan and B. J. Ingram, *J. Am. Chem. Soc.*, 2022, **144**, 14121–14131.

16 B. J. Kwon, S. H. Lapidus, J. T. Vaughey, G. Ceder, J. Cabana and B. Key, *Acc. Chem. Res.*, 2024, **57**, 1–9.

17 B. J. Kwon, K.-C. Lau, H. Park, Y. A. Wu, K. L. Hawthorne, H. Li, S. Kim, I. L. Bolotin, T. T. Fister, P. Zapol, F. K. Klie, J. Cabana, C. Liao, S. H. Lapidus, B. Key and J. T. Vaughey, *Chem. Mater.*, 2020, **32**, 1162–1171.

18 B. J. Kwon, L. Yin, H. Park, P. Parajuli, K. Kumar, S. Kim, M. X. Yang, M. Murphy, P. Zapol, C. Liao, T. T. Fister,

R. F. Klie, J. Cabana, J. T. Vaughey, S. H. Lapidus and B. Key, *Chem. Mater.*, 2020, **32**, 6577–6587.

19 P. Novak and J. Desilvestro, *J. Electrochem. Soc.*, 1993, **140**, 140–144.

20 L. Yu and X. Zhang, *J. Colloid Interface Sci.*, 2004, **278**, 160–165.

21 G. S. Gautam, P. Canepa, W. D. Richards, R. Malik and G. Ceder, *Nano Lett.*, 2016, **16**, 2426–2431.

22 S. H. Lee, R. A. DiLeo, A. C. Marschilok, K. J. Takeuchi and E. S. Takeuchi, *ECS Electrochem. Lett.*, 2014, **3**, A87–A90.

23 J. Yin, C. J. Pelliccione, S. H. Lee, E. S. Takeuchi, K. J. Takeuchi and A. C. Marschilok, *J. Electrochem. Soc.*, 2016, **163**, A1941–A1943.

24 S. Son, T. Gao, S. P. Harvey, K. S. Steirer, A. Stokes, A. Norman, C. Wang, A. Cresce, K. Xu and C. Ban, *Nat. Chem.*, 2018, **10**, 532–539.

25 K. W. Nam, S. Kim, S. Lee, M. Salama, I. Shterenberg, Y. Gofer, J.-S. Kim, E. Yang, C. S. Park, J.-S. Kim, S.-S. Lee, W.-S. Chang, S.-G. Doo, Y. N. Jo, Y. Jung, D. Aurbach and J. W. Choi, *Nano Lett.*, 2015, **15**, 4071–4079.

26 H. J. Lee, J. Shin and J. W. Choi, *Adv. Mater.*, 2018, **30**, 1705851.

27 M. Wang and S. Yagi, *J. Alloys Compd.*, 2020, **820**, 153135.

28 C. Miralles and R. Gómez, *Electrochem. Commun.*, 2019, **106**, 106512.

29 K. Shimokawa, T. Hatakeyama, H. Li and T. Ichitsubo, *Curr. Opin. Electrochem.*, 2023, **38**, 101209.

30 J. B. Goodenough and K. Park, *J. Am. Chem. Soc.*, 2013, **135**, 1167–1176.

31 J. B. Goodenough, *Acc. Chem. Res.*, 2013, **46**, 1053–1061.

32 A. Van der Ven, Z. Deng, S. Banerjee and S. P. Ong, *Chem. Rev.*, 2020, **120**, 6977–7019.

33 H. Wan, S. Li, X. Zhang, L. Wu, Z. Liu, G. Liu, C. Gao, W. Huang, H. Deng, W. Hu and F. Gao, *J. Phys. Chem. Lett.*, 2023, **14**, 10537–10544.

34 A. R. House, U. Maitra, M. A. Pérez-Osorio, J. G. Lozano, L. Jin, J. S. Somerville, L. C. Duda, A. Nag, A. Walters, Z. K. Zhou, M. R. Roberts and P. G. Bruce, *Nature*, 2020, **577**, 502–508.

35 X. Zhu, F. Meng, Q. Zhang, L. Xue, H. Zhu, S. Lan, Q. Liu, J. Zhao, Y. Zhuang, W. Guo, B. Liu, L. Gu, X. Lu, Y. Ren and H. Xia, *Nat. Sustain.*, 2021, **4**, 392–401.

36 S. Kumakura, Y. Tahara, K. Kubota, K. Chihara and S. Komaba, *Angew. Chem., Int. Ed.*, 2016, **55**, 12760–12763.

37 H. Kim, D. Seo, J. Kim, S. Bo, L. Liu, T. Shi and G. Ceder, *Adv. Mater.*, 2017, **29**, 1702480.

38 R. Luo, X. Li, J. Ding, J. Bao, C. Ma, C. Du, X. Cai, X. Wu and Y. Zhou, *Energy Storage Mater.*, 2022, **47**, 408–414.

39 J. Weng, J. Duan, C. Sun, P. Liu, A. Li, P. Zhou and J. Zhou, *Chem. Eng. J.*, 2020, **392**, 123649.

40 W. Zuo, J. Qiu, X. Liu, B. Zheng, Y. Zhao, J. Lia, H. He, K. Zhou, Z. Xiao, Q. Li, G. F. Ortiza and Y. Yang, *Energy Storage Mater.*, 2020, **26**, 503–512.

41 W. Sun, L. Chen, J. Wang, H. Zhang, Z. Quan, F. Fu, H. Kong, S. Wang and H. Chen, *J. Mater. Chem. A*, 2023, **11**, 15724–15731.